Photoconductivity studies of treated CdSe quantum dot films exhibiting increased exciton ionization efficiency

M. V. Jarosz,[1,2] V. J. Porter,[1,2] B. R. Fisher,[1,2] M. A. Kastner,[1,3] and M. G. Bawendi[1,2]
[1]*Center for Materials Science and Engineering, Massachusetts Institute of Technology, Cambridge, Massachusetts 02139, USA*
[2]*Departments of Chemistry, Massachusetts Institute of Technology, Cambridge, Massachusetts 02139, USA*
[3]*Department of Physics, Massachusetts Institute of Technology, Cambridge, Massachusetts 02139, USA*
(Received 16 April 2004; revised manuscript received 7 September 2004; published 18 November 2004)

We present measurements of photoconductivity in CdSe quantum dot films treated with a variety of reagents. While the photocurrent of untreated samples is highly voltage dependent at all voltages, after treatment the photocurrent is much larger, depends strongly on voltage at low voltage, displays a linear region above a voltage threshold, and finally saturates at high voltage. All regions of the current-voltage curves after treatment can be reproduced with a model that requires noninjecting contacts and a field dependent exciton ionization efficiency that saturates to unity. This model is shown to be consistent with the trends observed with different treatments. The changes in photocurrent with treatment are shown to be largely a consequence of increased quantum dot surface passivation and decreased quantum dot spacing, regardless of whether the molecules used for treatment are conjugated or able to cross-link the quantum dots.

DOI: 10.1103/PhysRevB.70.195327 PACS number(s): 73.63.Bd, 73.63.Kv, 72.40.+w

I. INTRODUCTION

Semiconductor quantum dots (QDs) are of interest because of their tunable optical and electronic properties and their applications as novel materials for biological imaging,[1–5] light emitting diodes,[6–9] photovoltaics,[10–12] photodetectors,[13,14] and lasers.[15,16] Colloidal nanocrystals are of particular interest because of the ease with which they can be synthesized, manipulated, and assembled into device structures. Many of the applications of colloidal QDs involve charge transport, and recent experiments have underscored the important role that charges play in the optical properties of colloidal quantum dots.[17–20] Furthermore, the motion of electrons in QD arrays is interesting because one can think of the system as an artificial solid composed of artificial atoms.[21] Because of localization of electrons on the QDs, strong correlations are expected in the motion of charge carriers. However, because dark conductances are found to be extremely small in uncharged quantum dot arrays, photoconductivity is the best way to study electronic motion in these systems.

Enhancing the photoconductivity in QD films would advance both the understanding of the physics of charges in QDs and the realization of QD applications. Until now, an increase in the photoconductivity has only been achieved by annealing QD films at temperatures high enough to decompose the QD capping layer.[22] The dark conductivity of QD films in an electrochemical cell has, however, been shown to increase upon treatment with diamine cross-linking.[23,24] In this paper, we present a set of postdeposition chemical treatments that increase the photoconductivity in CdSe QD films by orders of magnitude. We show that the photoconductivity in CdSe QD films can be enhanced by treatment with amines or a strong base. While the untreated samples show a photocurrent that is highly voltage dependent at all voltages, such behavior is observed only at low voltages for the samples treated with amines or sodium hydroxide; at higher voltages, the photocurrent becomes linear with voltage. For samples exhibiting the greatest enhancement following treatment, the photocurrent also exhibits saturation at very high voltage. We present a model that is able to explain all three regimes of voltage dependence in the treated samples by assuming: noninjecting contacts and an ionization efficiency that is highly voltage dependent and that saturates at unity at the voltage for which the current-voltage (i-V) curve becomes linear. As well as predicting the trends observed in the voltage dependence of the photocurrent, our model also predicts that the product of the mobility and lifetime for electrons is probably not more than $\sim$10 times greater than the product for holes. We show that the main parameters leading to the increase in photoconductivity are the degree of surface passivation and the spacing between QDs. Whether or not the molecules used to treat the films are conjugated or are able to cross-link the QDs do not appear to be significant factors.

II. EXPERIMENTAL DETAILS

A. Sample preparation

CdSe QDs with a diameter of 40 Å are synthesized using a method based on a cadmium salt precursor.[25] A cadmium precursor solution consisting of cadmium hydroxide (98%), tri-*n*-octylphosphine (TOP, 90%), and *cis*-9-octadecenoic acid (99%) is degassed under vacuum for 1 h. After cooling to room temperature, the selenium precursor, tri-*n*-octylphosphine selenide (TOPSe, 1.5 M solution), is added and the precursors are injected into a 335 °C coordinating solvent solution containing TOP, oleylamine, and dioctyl ether. Upon cooling, butanol is added to the growth solution.

An aliquot of the growth solution is removed and processed following previously established procedures for making close-packed films.[26–32] These procedures narrow the size distribution and remove excess organics that would inhibit formation of an optically clear and close-packed film.

After an initial precipitation with methanol, the precipitate is dissolved in hexane and placed in the freezer for 10 min to encourage precipitation of salts. The sample is then centrifuged and butanol is added to the supernatant. This solution is passed through a 0.2 μm filter and a second precipitation is carried out with methanol. The resulting precipitate is dissolved in hexane and butanol, passed through a 0.1 μm filter, and a final precipitation with methanol is performed. The final precipitate is dissolved in hexane and dried under vacuum. The powder of QDs is dissolved in a 9:1 mixture of hexane:octane, filtered through a 0.02 μm filter, and dried under vacuum once again. The QD powder is then brought into an inert atmosphere glovebox, where it is redissolved in 9:1 hexane:octane. Films are deposited by drop-casting this solution onto lithographically patterned silicon substrates.

The silicon devices are fabricated by thermally growing 330 nm of oxide on degenerately doped silicon substrates and patterning $200\times800\times0.1$ μm^3 gold bar electrodes using a standard lift off procedure.[33] The spacing between electrodes is 1 μm. The devices are mounted on chip carriers, and electrical contacts from the electrodes to the chip carrier are made prior to film deposition.

B. Conductivity measurements

All photoconductivity measurements are carried out under vacuum in a Janis VPF-100 cryostat. The 514 nm line of an Ar^+ laser is used to excite the samples. The laser beam with an intensity of ~14 mW/cm^2 (unless otherwise stated) is focused onto a pair of gold electrodes. It has been shown in a previous study that photocurrent is not due to photoinjection from the gold electrodes.[26] Current measurements are made with a Keithley 6517 electrometer, which also supplies the source-drain voltage. For the photocurrent versus voltage curves, the voltage is stepped in 2 V increments from 0 V to 20 V, and in 10 V increments from 20 V to 100 V. The data points are recorded after a delay of 10 s. Unless otherwise stated, the data are taken with the sample at 77 K.

C. Treatment

After measuring the photoconductivity of a QD film, the sample is returned to the glovebox where it is immersed in a 0.1 M solution of the selected reagent: butylamine, aniline, 1,6-diaminohexane, 1,4-phenylenediamine, tri-*n*-butylphosphine, or sodium hydroxide. The solvent for each solution is anhydrous acetonitrile, except for sodium hydroxide which is dissolved in anhydrous methanol due to its limited solubility in acetonitrile. The sample is soaked for 10 min, rinsed with 1 mL of solvent, and dried in an oven at 70 °C for 1 h to remove excess solvent.[24] Two types of butylamine-treated samples are presented: one dried in the oven and the other dried in the glovebox overnight. For all samples other than the one dried overnight, reference and treated devices were measured on the same day.

D. Transmission electron microscopy

The spacing between close-packed QDs in the reference samples is found using transmission electron microscopy (TEM). Samples are prepared by drop casting a solution of QDs onto a carbon TEM grid. The solution is $\sim$200 times more dilute than the solution used to make films in order to form a monolayer of QDs. The sample is imaged on a JEOL 200CX electron microscope under 100 000 times magnification. After averaging the QD spacing for over 90 QDs, the interdot spacing in the pretreated films was determined to be 1.1 nm$\pm$0.3 nm, which is consistent with previous studies.[32]

E. Atomic force microscopy

Sample thicknesses are measured using atomic force microscopy (AFM), with a Digital Instruments Nanoscope IIIa in D3000 tapping mode. AFM samples are prepared in the same manner as the samples used for electrical measurements, except that they are deposited in air onto clean glass slides. The sample is scratched down to the glass to remove the QD film from a small region of the sample. A $30-50$ μm$\times30-50$ μm region, half over the glass slide and half over the film, is scanned by the AFM, allowing a calculation of the average height of the film relative to the glass slide. Heights are measured in three separate regions on each sample. After chemical treatment, the average height of the film is measured in the same regions. As the size of the CdSe core does not change, the decrease in the thickness of the films is due to a decrease in QD spacing after treatment with 1,4-phenylenediamine, 1,6-diaminohexane, aniline, or tri-*n*-butylphosphine. The analysis is less straightforward after treatment with butylamine and sodium hydroxide, because some of the film is redissolved so interparticle spacing is only given by glancing angle x-ray scattering measurements.

F. Glancing angle x-ray scattering (GAXS)

GAXS is also used to obtain changes in relative interparticle spacing after chemical treatments. Measurements are performed on a Rigaku 300 Rotaflex diffractometer with a 185 mm focusing circle in glancing angle mode. In glancing angle mode only the x-ray detector is rotated while the sample is held at a small incident angle. GAXS assists in the analysis of thin films as the small incident angle limits diffraction to points on the surface of the film, keeping the peak to background ratio high.

Samples are prepared in the same manner as for electrical and AFM measurements differing only in that samples are deposited in air on clean pieces of silicon. The samples are then chemically treated. For the GAXS measurements, the accelerating voltage on the copper anode is 60 kV and the flux is 300 mA. The incident angle is set to an angle between 1° and 2° depending on the exact position of the sample in its holder. The detector continuously scans 2θ from 1.7° to 7° at a rate of 0.8° per min and collects data every 0.02°.

G. Fluorescence microscopy

Fluorescence microscopy is used to study fluorescence quenching as a function of applied voltage in the electrically active portion of the QD film. The device structure is the same as that used for the photoconductivity measurements. A homebuilt epifluorescence, wide field microscope is used to

image inside a cold finger cryostat with a 0.7 mm thick window. The objective is a 60×0.7 NA DIC Nikon objective with a working distance of ~2 mm, with the correction collar set to 0.75 mm. The excitation source is an Ar^+ laser operating at 514 nm and ~300 W/cm^2. Collection of the fluorescence is passed through a 514 nm notch filter and a dielectric bandpass filter to eliminate excitation light from the collected path. This collected light is then imaged on a 1024×1024 pixel CCD detector (Princeton Instruments Micromax, Roper Scientific).

III. RESULTS

Figures 1 and 2 are photo-induced current versus voltage (*i-V*) curves for films of CdSe QDs measured at 77 K. Each *i-V* curve is scaled to display the untreated (reference) and treated films on the same plot. The photocurrent of the reference sample is designated as i_r, and the photocurrent after treatment is designated as i_t. The lines connecting the data points serve only as a visual aid. In each figure the current for the reference is highly nonlinear in voltage over the entire range. The currents at 50 and 100 V are typically on the order of 0.1–1 pA and 5–50 pA, respectively. The dark current from 0 to 100 V is below the noise (<0.1 pA) for all reference and treated samples. An example of the dark current before and after treatment with butylamine is displayed in Fig. 3. These results agree well with those found in previous studies of photoconductivity in CdSe QD films.[22,26,30,34]

Inter particle spacing found using AFM and GAXS is summarized in Table I. The raw data from GAXS is displayed in Fig. 4(a). Previous studies showed that the first peak in the GAXS scan results from interference between QDs and gives information about interparticle spacing.[29] Subsequent peaks are a result of atomic scattering. To obtain the interparticle spacing the background is subtracted from the total intensity to extract the structure factor, $S(q)$. The structure factor can be Fourier transformed using Eq. (1) to find the pair distribution function, $g(r)$,

$$g(r) = 1 + \frac{1}{2\pi^2 r\rho_o}\int_0^\infty [S(q)-1]q\sin(qr)W(i)e^{-\alpha^2q^2}dq. \tag{1}$$

In Eq. (1) r is distance in angstroms, ρ_o is the average electron density, and $q=4\pi\sin\theta/\lambda$, where λ is the wavelength of the x rays (1.54 Å) and θ is half the angle measured by GAXS. As $S(q)$ is a finite data set a convergence factor, $e^{-\alpha^2q^2}$, is added to minimize false features resulting from early termination.[35] A step function, $W(i)$, has also been included to isolate the first peak from those resulting from atomic scattering. The pair distribution functions for the reference and treated samples are presented in Fig. 4(b). The diameter of the CdSe QD core is determined from the position of the first peak in the absorbance spectrum and found to be 40 Å.[27]

The *i-V* curve shown in Fig. 1(a) is for a sample treated with butylamine, an unconjugated molecule with a single amine group; this sample was dried overnight at room temperature. Upon treatment the photoconductivity increases 82-fold at 100 V and 310-fold at 50 V. In addition, the shape of the *i-V* curve after treatment becomes linear above ~60 V.

When a sample is treated with butylamine and dried in the oven at 70 °C, as opposed to drying at room temperature overnight, there is a much larger increase in the photoconductivity. Figure 1(b) shows a 145-fold increase in photocurrent at 100 V and a 1280-fold increase at 50 V. As in Fig. 1(a), the *i-V* curve in Fig. 1(b) also shows a transition to a linear regime; however, this transition occurs at ~14 V. Furthermore, saturation of the photocurrent is evident in Fig. 1(b), above ~70 V. Analysis of GAXS data shows that QDs in butylamine treated films are brought 2.7 Å closer together when dried at an elevated temperature rather than dried at room temperature overnight.

Figure 1(c) displays the results for treatment with aniline, a conjugated molecule with one amine group. The photocurrent increases threefold at 100 V upon treatment and sixfold at 50 V. The initial photocurrent is somewhat higher than for the other samples. Nonetheless, the shape of the reference curve is nonlinear over the entire voltage range, whereas the treatment induces a linear regime above ~60 V. The magnitude of the photocurrent at 100 V is hundreds of picoamps, similar to Figs. 1(a), 1(d), and 1(f). GAXS data suggests that the spacing between QDs after treatment with aniline is ~6.8 Å.

Figure 1(d) shows the result of treatment with a shorter analog of TOP, tri-*n*-butylphosphine (TBP). GAXS data suggests that the QD spacing after treatment with TBP is 6.8 Å, which is identical to the spacing of the aniline-treated sample in Fig. 1(c). Both samples have photocurrents on the order of hundreds of picoamps at 100 V. However, the shape of the *i-V* curve for the TBP-treated sample does not show a linear region like that of the sample treated with aniline.

Figure 1(e) is data for a sample treated with 1,6-diaminohexane, an unconjugated diamine. At 100 V, the conductivity of the treated sample has increased 33-fold over that of the reference and at 50 V it has increased 225-fold. The shape of the 1,6-diaminohexane treated *i-V* curve is similar to those of the butylamine-amine treated samples in that there is a clear linear region. For the former, the linear region begins at ~30 V. There is also evidence of photocurrent saturation beginning above ~80 V. The magnitude of the photocurrent at 100 V is on the order of hundreds of picoamps, similar to that of the sample treated with butylamine and dried overnight. GAXS data shows that after treatment with 1,6-diaminohexane the QD spacing is ~4.1 Å.

Treatment with 1,4-phenylenediamine, a conjugated diamine, also shows an increase in photoconductivity. However, the magnitude of the photocurrent at 100 V is less than for treatment with aniline, 1,6-diaminohexane, or butylamine. Figure 1(f) shows an 11-fold increase in photocurrent at 100 V, a 36-fold increase at 50 V, and the onset of a linear response at 60 V. Interdot spacing after this treatment is ~7.5 Å, slightly larger than the aniline-treated sample.

The reason amines increase the photocurrent may be attributed to their basic and passivating nature, as discussed below. Therefore, treatment with a very small and strong

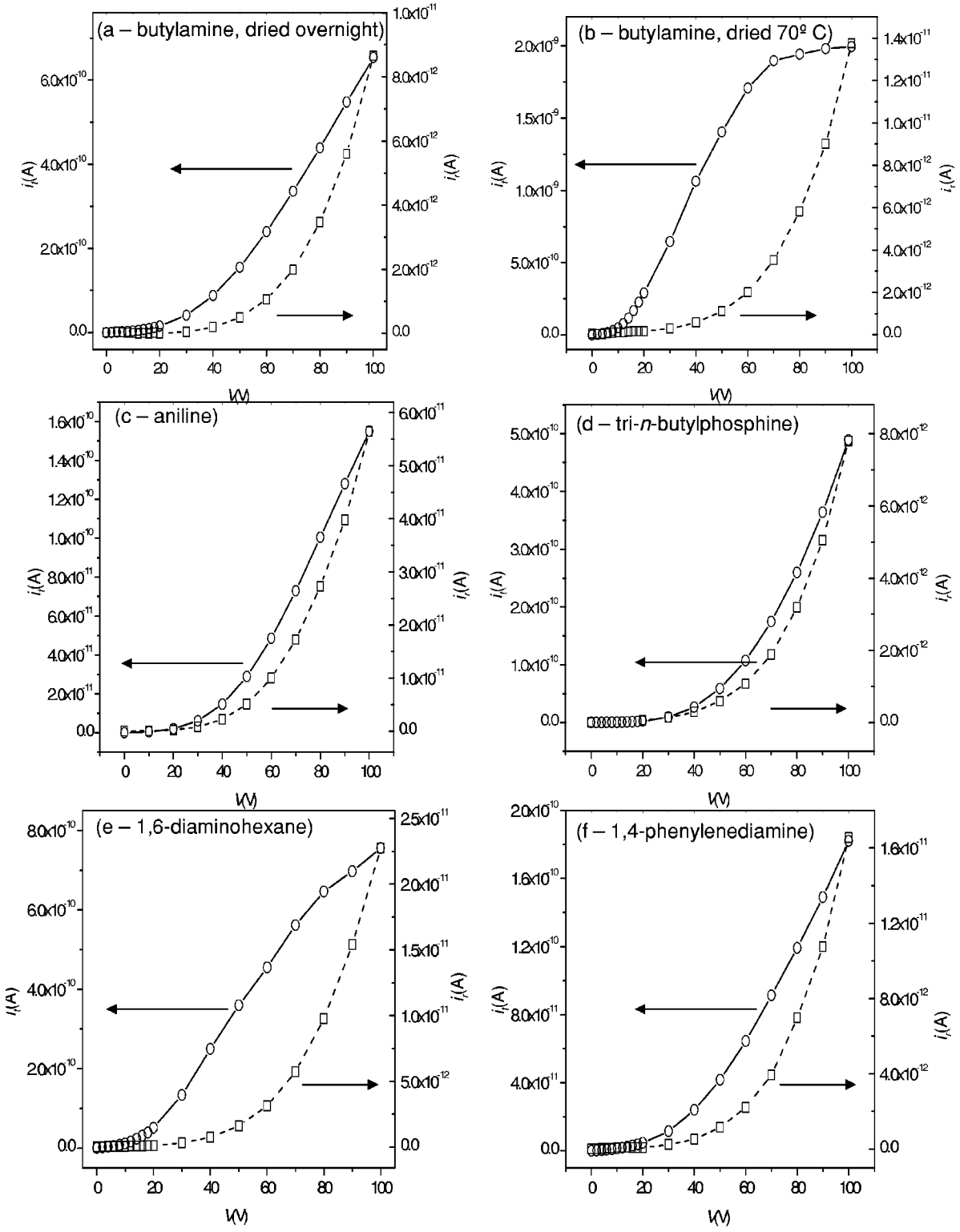

FIG. 1. Photocurrent at 77 K before (open squares, dashed line) and after (open circles, solid line) treatment with (a) butylamine (dried at room temperature overnight), (b) buytlamine (dried at 70 °C for 1 h), (c) aniline, (d) tri-*n*-butylphosphine, (e) 1,6-diaminohexane, and (f) 1.4-phenylenediamine.

base, also known to increase photoluminescence quantum yield,[36] should increase photoconductivity as well. Figure 2 shows the result of treatment with sodium hydroxide. The photocurrent increases by a factor of 440 at 100 V and by a factor of 5100 at 50 V. The shape of the *i-V* curve resembles that of the sample treated with butylamine (oven-dried) in that it has a linear region followed by saturation. In addition GAXS shows that QDs are 0.6 Å apart, even closer than the butlyamine (oven-dried) sample. The linear region starts at ~18 V, and the current is on the order of nanoamps.

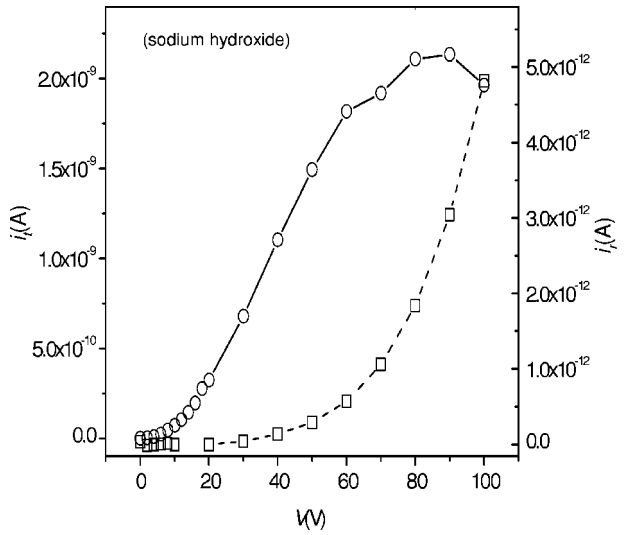

FIG. 2. Photocurrent at 77 K before (open squares, dashed line) and after (open circles, solid line) treatment with sodium hydroxide.

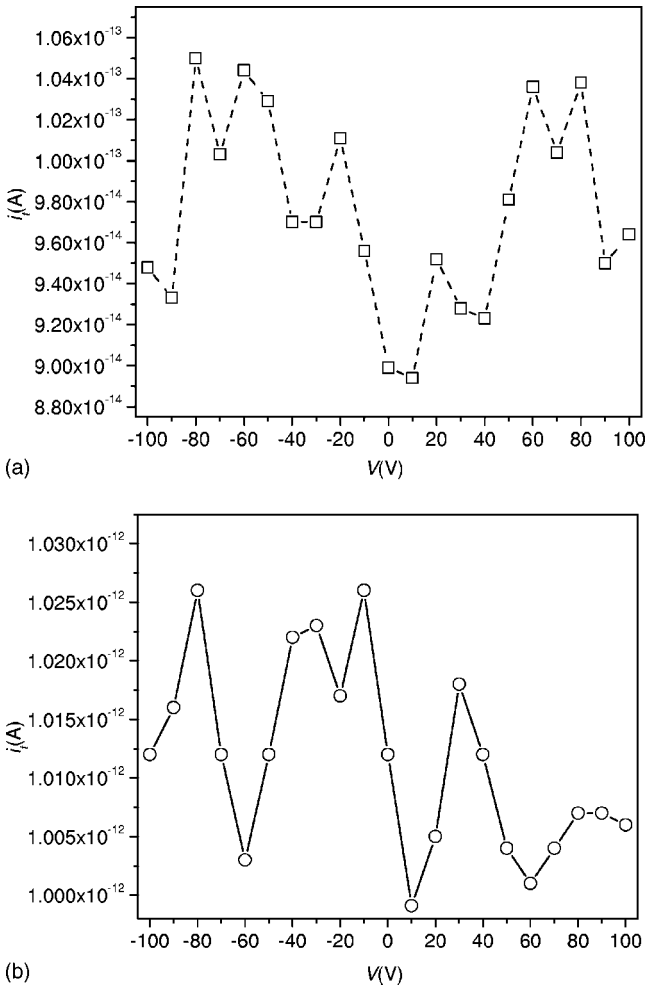

FIG. 3. Dark current at 77 K (a) before (open squares, dashed line) and (b) after treatment with butylamine and drying at 70 °C for 1 h (open circles, solid line).

TABLE I. Interparticle spacing from AFM and GAXS for the reference and treated samples.

Treatment	Interparticle spacing AFM (Å)	GAXS 2 theta (°) ±0.02°	Interparticle spacing GAXS (Å)
Reference		2.10	11.0±0.3
1,4-phenylenediamine	5–7	2.22	7.5±0.3
Aniline	5–7	2.30	6.8±0.3
Tri-*n*-butylphosphine	7	2.30	6.8±0.3
Buytlamine (dried overnight)	5–7	2.37	4.6±0.3
1,6-diaminohexane	3–5	2.48	4.1±0.3
Butylamine (oven-dried)		2.60	1.9±0.3
Sodium hydroxide		2.64	0.6±0.3

Figure 5 shows the photocurrent intensity dependence for a sample treated with sodium hydroxide at a voltage corresponding to photocurrent saturation. The current is linear in intensity to within the error.

The open circles in Fig. 6 represent the low voltage portion of the *i*-*V* curve for the butylamine-treated sample which is dried at 70 °C; the full *i*-*V* curve for the same sample is shown in Fig. 1(b). The solid line in Fig. 6 represents the photocurrent of the untreated sample, scaled in voltage and current to demonstrate that the shape of the *i*-*V* curve for the treated sample in the low voltage regime is the same as the shape of the reference *i*-*V* curve at all voltages. The nonlinear portion of the *i*-*V* curve at low voltages is not significantly altered by any of the treatements.

Figure 7(a) shows the correlation between the photoconductivity and photoluminescence of a sample treated with 1,6-diaminohexane. The *i*-*V* curve for the sample (solid line, open circles) is plotted in conjunction with fluorescence quenching data (solid squares). ΔI_F represents the change in fluorescence intensity when the electric field is applied. Because of a high level of background fluorescence, it is not possible to determine a quantitative value for the percent fluorescence quenching. The white region of Fig. 7(a) represents the voltage range over which the *i*-*V* curve exhibits highly voltage dependent behavior, and the white-gray boundary is approximately where the *i*-*V* curve becomes linear. The degree of fluorescence quenching increases quickly when the voltage becomes high enough for the *i*-*V* curve to become linear and then saturates. Figure 7(b) demonstrates that while no significant fluorescence quenching is observed when +20 V is applied, a distinctive and reversible fluorescence quenching is observed when +100 V is applied.

Figure 8(a) shows the *i*-*V* curves for a reference sample at 77 K and 300 K; the photocurrent at 100 V is more than 30 times smaller at 300 K than at 77 K, consistent with previous observations.[26] Figure 8(b) shows the *i*-*V* curves for a sample treated with butylamine and oven-dried, taken at 77 K and 300 K; the photocurrent at 100 V is only about 5 times smaller at 300 K than at 77 K. The photocurrent at

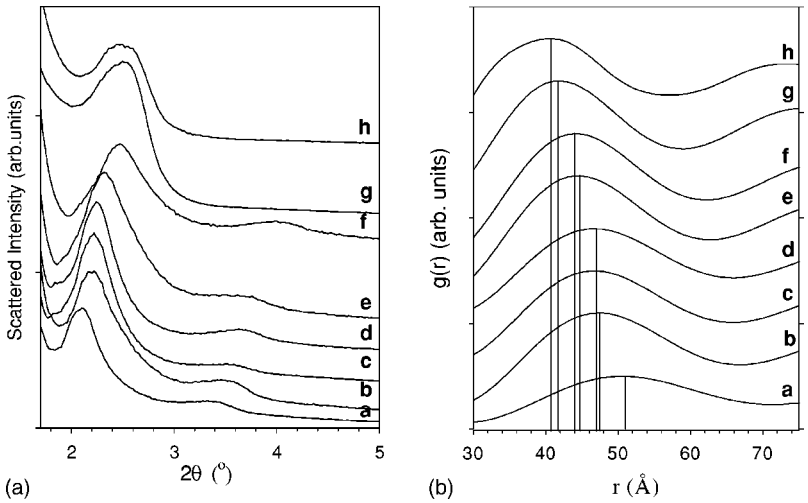

FIG. 4. (a) GAXS raw data for **a** reference, **b** 1,4-phenylenediamine, **c** aniline, **d** tri-*n*-butylphosphine, **e** butylamine (dried at room temperature overnight), **f** 1,6-diaminohexane, **g** butylamine (dried at 70 °C for 1 h), **h** sodium hydroxide. Data are offset for clarity. (b) The pair distribution function $g(r)$ for the reference and treated samples. The solid line marks the center of the peak and the labels are the same as in (a).

300 K still reaches a linear regime, although not until a higher voltage. Furthermore, while the treated *i-V* curve at 77 K saturates at 90 V, at 300 K saturated photocurrent is not observed in the range of voltages that are measured.

IV. DISCUSSION

A comparison of the *i-V* curves in Figs. 1(a)–1(f) and 2 suggests that two phenomena increase photoconductivity and affect *i-V* curve shapes: QD spacing, and the functionality of the reagent used for treatment. Amine functionality is expected to passivate recombination centers at the QD surface. This idea is supported by the observation that amines are known to increase the photoluminescence quantum yield of QDs.[25,37–40] The increase in photoconductivity for the TBP-treated sample is predominantly caused by the decrease in QD spacing, whereas the increase for the aniline treated sample probably results from both a decrease in QD spacing and an increase in surface passivation.

It has been suggested that the use of cross-linking molecules can improve the conductivity of QD films.[23,24] While the photoconductivity does improve with 1,6-diaminohexane, shown in Fig. 1(e), it increases with butylamine as well. Furthermore, the QDs are 0.5 Å closer together after the 1,6-diaminohexane treatment compared to the butylamine (dried overnight) treatment, so it does not appear that cross-linking has a significant impact, compared with surface passivation and QD spacing.

From the shape of the *i-V* curve and the magnitude of the photocurrent in Fig. 1(c), after treatment with aniline, it appears that conjugation also does not affect the photoconductivity as much as passivation and QD spacing. In fact, aniline may have less of a passivating effect than 1,6-diaminohexane or butylamine because its bulkier phenyl group may inhibit surface binding. In addition, if conjugation or cross-linking were responsible for the increase in photoconductivity, treatment with 1,4-phenylenediamine should have displayed the greatest improvement. The fact that the photoconductivity does not increase dramatically, as seen in Fig. 1(f), strength-

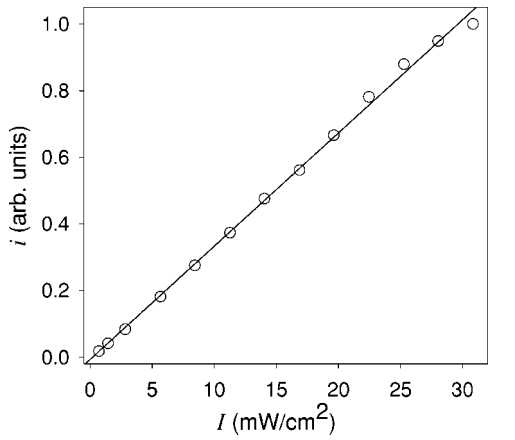

FIG. 5. Intensity dependence of the photocurrent for a sample treated with sodium hydroxide at 100 V, after the photocurrent has saturated with voltage. Open circles represent data and the solid line represents a linear fit.

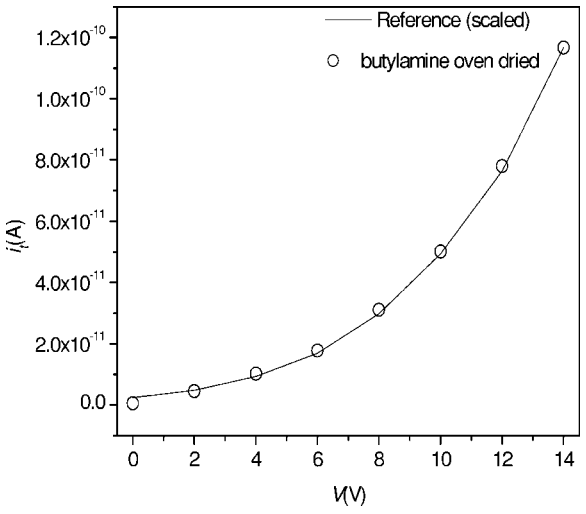

FIG. 6. Photocurrent data (open circles) for a sample treated with butylamine and dried at 70 °C for 1 h, plotted with reference data (solid line). The current and voltage values for the reference data are scaled to illustrate that the shape of the butylamine treated *i-V* curve, at low voltages, is the same as the shape of the reference at all voltages.

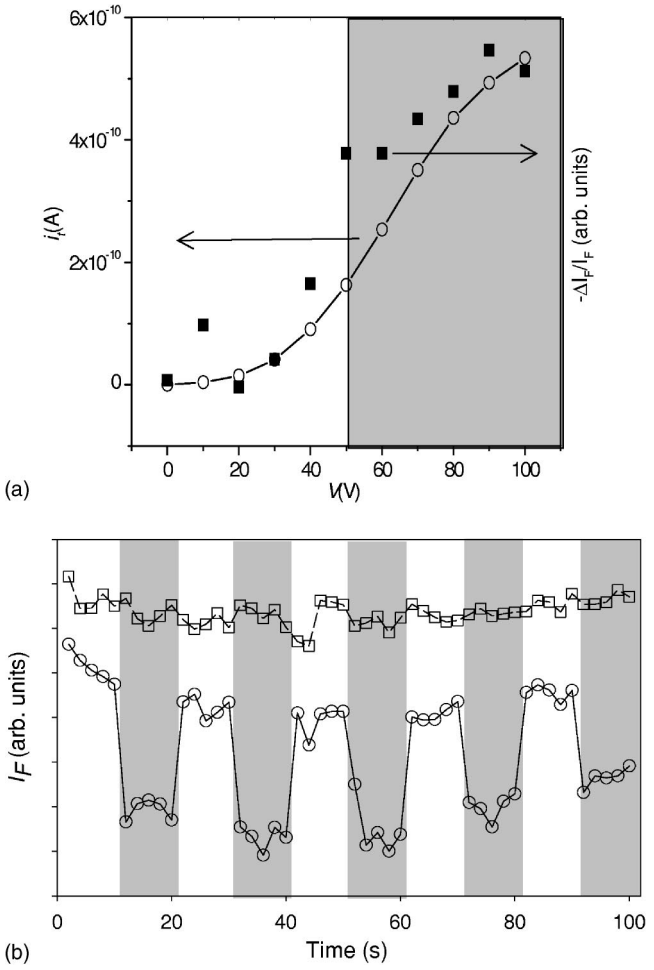

FIG. 7. (a) Fluorescence quenching data (filled squares) for a sample treated with 1,6-diaminohexane compared to the *i-V* curve (open circles, solid line) for the same sample. The shaded region contains voltages at which the *i-V* curve is linear and a saturated exciton ionization efficiency is predicted. (b) Time trace of the fluorescence intensity for the same sample as in (a) where the white region corresponds to 0 V and the shaded region corresponds to +20 V (open squares, dashed line) or +100 V (open circles, solid line). The curves corresponding to +20 V and +100 V are offset for clarity. A quantitative number for the percent fluorescence quenching in (a) and (b) was not obtainable due to high background fluorescence.

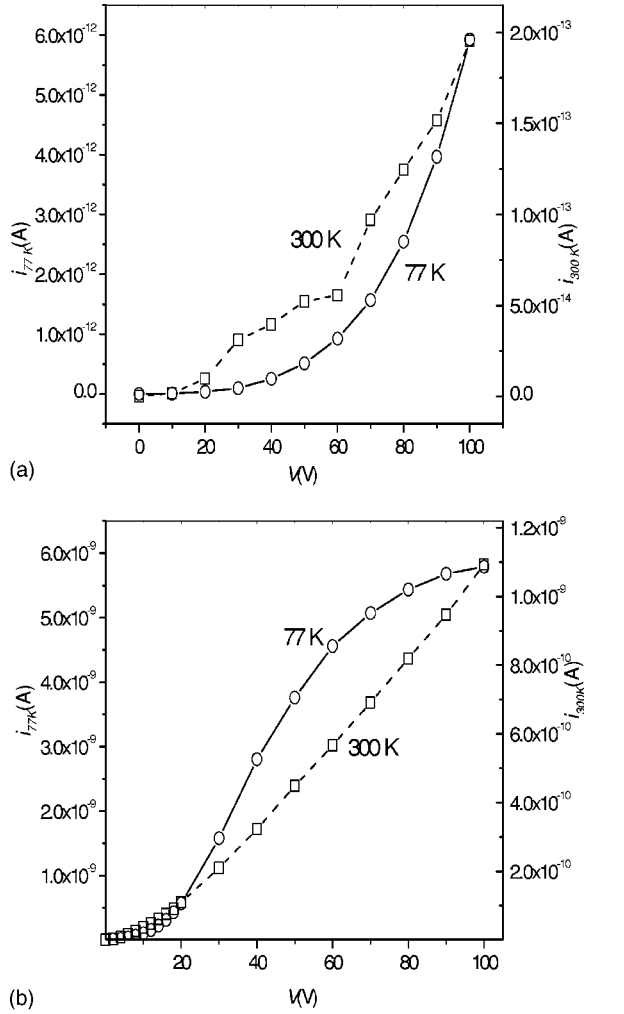

FIG. 8. (a) Photocurrent before treatment at 77 K (open circles, solid line) and 300 K (open squares, dashed line). (b) Photocurrent after treatment with butylamine (oven-dried) at 77 K (open circles, solid line) and 300 K (open squares, dashed line).

ens the argument that surface passivation and QD spacing, rather than conjugation or cross-linking, are responsible for the larger photocurrents and the changes in the *i-V* curve shapes.

The similarities between the results obtained after treatment with sodium hydroxide and after treatment with butylamine (oven-dried) suggest a similar mechanism by which the photocurrent is improved. The major difference between treatment with sodium hydroxide or butylamine (oven-dried) and treatment with the other four amines is the degree to which the QD spacing is decreased.

Previous studies[26] have established that photoconduction in CdSe QD films is limited by field-induced ionization of photo-generated excitons; the majority carrier is assumed to be the electron. The exciton ionization process requires an electron to tunnel to a neighboring QD, and thus is highly dependent on voltage. A model for this voltage dependence has been previously proposed.[26] The shapes of the reference *i-V* curves seen in Figs. 1, 2, 6, and 8 correspond well to those previously reported, where the highly voltage dependent *i-V* curve is attributed to the voltage dependence of exciton ionization.

The most obvious change in the voltage dependence of the *i-V* curves upon treatment with reagents is seen in Figs. 1(b) and 2, the sample treated with butylamine and dried at 70 °C, and the sample treated with sodium hydroxide, respectively. For these, the photocurrent saturates to a constant value at high voltages. In traditional photoconductors, such a saturation of photocurrent with voltage is seen when both the minority and majority carriers are mobile but it is not possible to inject either carrier from the electrodes.[41,42] The contacts in this situation are referred to as blocking,[43] and photocurrent is maintained by carriers being extracted at the electrodes. The photocurrent under these circumstances is referred to as primary photocurrent[41,44] because it comes only from carriers generated within the sample.

It is not surprising that the contacts are blocking. From previous dark conductivity studies one knows that it is difficult to inject electrons into the conduction band and nearly impossible to inject holes into the valence band of a CdSe QD from a gold electrode.[22,33,45] Figures 3(a) and 3(b) are *i-V* curves in the dark from ±100 V. Any dark current is lost in the noise and less than 0.1 pA. The difficulty to inject electrons can be explained by the positions of the conduction and valence states of CdSe QDs with respect to the Fermi level of gold: for 4 nm diameter CdSe QDs, the conduction state is ~0.5 eV above and the valence state is ~1.6 eV below the Fermi level of gold.[9,45,46]

Complete saturation of the photocurrent occurs at voltages that are high enough that the following requirements are met: carriers are extracted rapidly enough that there is no recombination of either carrier within the film, and the generation rate does not depend on the field. Thus, the electron and hole lifetimes are transit-time limited, rather than being recombination-time limited. When the photocurrent saturates, the photoconductive gain, G, becomes equal to unity. This can be seen from the following equation for photoconductive gain, which is valid for primary photoconductors:[41,44]

$$G = \frac{l_p + l_n}{L}, \tag{2}$$

where L is the distance between the electrodes, and l_p and l_n are the distances traveled by the hole and electron, respectively, before recombination, trapping, or arrival at an electrode. Since L is the maximum value for $l_p + l_n$, the maximum value for the photoconductive gain, G, is 1.[41]

The photocurrent, i, is related to G as follows:[41]

$$i = eGF, \tag{3}$$

where e is the charge of an electron and F is the number of free carriers (ionized excitons) created per second by photoexcitation anywhere in the sample. Thus we interpret the saturation of the photocurrent as a saturation of G at $G=1$.

In the saturation regime of the *i-V* curve we can determine the value of F for $G=1$, F_{sat}. Whether or not this value is reasonable given the photoexcitation intensity and QD film absorption serves as a check on the applicability of the model. To experimentally determine the photon absorption, a thin film of CdSe QDs is deposited on a glass slide and treated with butylamine; the thickness after treatment is determined by AFM to be 45 nm, and the optical density is determined to be 0.027 at 514 nm. The height of the QD film used in the *i-V* measurements is 100 nm. The optical density found above from the 45 nm thick film corresponds to a 100 nm thick film having an optical density of 0.06 at 514 nm. Based on the data in Fig. 1(b) or Fig. 2, F_{sat} is calculated to be $\sim 1.3 \times 10^{10}$ electrons per second. Using Eq. (4) given the excitation intensity of 1 mW, the active area between the electrodes, and assuming one carrier per absorbed photon (assuming an ionization probability of $S=1$), the above value of F_{sat} leads to an absorption, A, of ~0.13. This corresponds to an optical density of ~0.06, consistent with the direct measurement of absorption.

In addition to explaining the saturation of the photocurrent with voltage, Eq. (3) also predicts that the photocurrent in the saturation regime should be linear with intensity, since F_{sat} depends linearly on intensity [see also Eq. (4) below]. The expected linear dependence is seen in Fig. 5.

There is a significant difference between the photoconductivity of the amine- and base-treated CdSe QD films at low voltages and at high voltages. As is seen in Fig. 6 (the *i-V* curve for a sample treated with butylamine and dried at 70 °C), at low voltages the photocurrent has the same strong dependence on voltage that is present at all voltages for the reference sample. This voltage dependence has been previously ascribed to the highly voltage dependent nature of exciton ionization efficiency.[26] However, to observe saturation of the photoconductivity at high voltages, F must be voltage independent. The rate of carrier generation in the entire sample is

$$F = I \cdot A \cdot S, \tag{4}$$

where I is the intensity in units of photons per second, A is the absorption in units of excitons per photon, and S is the ionization efficiency in units of separated electrons per exciton ($0 \leqslant S \leqslant 1$). Since F is constant and S is monotonically increasing with field, we must have $S=1$ in the saturation regime.

In fact, the existence of a linear regime in the *i-V* curves of all of the amine- and base-treated samples is also consistent with $S=1$. In steady state the photocurrent can be written as

$$i = (\tau_n \mu_n + \tau_p \mu_p) e \frac{V}{L^2} \cdot F, \tag{5}$$

where τ_n and τ_p are the lifetimes of the electron and hole, respectively, μ_n and μ_p are the electron and hole mobilities, respectively, and V is the applied voltage. This equation predicts a linear voltage dependence if F (and therefore S) is field independent. In the low-voltage regime (and at all voltages for the reference samples), where S (and therefore F) has a strong field dependence, the photocurrent becomes similarly strongly dependent on voltage.

The slope of the linear region in the *i-V* plot is $\{[(\tau_n \mu_n + \tau_p \mu_p) e \cdot F]/L^2\}$. F is equal to F_{sat} as $S=1$ in the linear region, and e and L are known. Therefore, fitting the slope of the *i-V* curve allows $(\tau_n \mu_n + \tau_p \mu_p)$ to be extracted. For the butylamine sample dried in the oven shown in Fig. 1(b), $F_{sat} \sim 1.3 \times 10^{10}$ electrons per second. Fitting a line to the linear region gives $(\tau_n \mu_n + \tau_p \mu_p) \sim 1.8 \times 10^{-10}$ cm^2 V^{-1}. In the linear region every exciton is separated but the electron and hole recombine before reaching the electrodes. Thus τ_p and τ_n are both equal to the recombination time. The recombination time must be faster than 10 s (data points were taken every 10 s) or else the linear region would have not been observed. The graph would have transitioned directly from the highly voltage dependent region to saturation. Setting τ_p and τ_n equal to 10 s gives a lower bound for $(\mu_n + \mu_p)$ of 1.8×10^{-11} cm^2 V^{-1} s^{-1}.

The above model predicts that at voltages where the *i*-*V* curve becomes linear, a drop in fluorescence intensity should be observed from the QDs between the electrodes because excitons ionize rather than recombining in the QDs. Furthermore, the amount of fluorescence quenching should saturate to a constant value at these voltages. This is not inconsistent with the data of Fig. 7.

In fact, Eq. (5) is an oversimplification. While it can predict the general trends of the observed *i*-*V* characteristics (highly voltage dependent, then linear, then saturated), it cannot explain why the linear portions of the *i*-*V* curves do not extrapolate to zero applied field at zero photocurrent. We show that this discrepancy is a direct consequence of having a field dependent ionization efficiency at low voltages and of having blocking contacts. Were S constant, the *i*-*V* curves would simply be linear at low voltages and would saturate at high voltages when $G=1$.

Blocking contacts lead to the accumulation of charge near each electrode. In the case of CdSe QDs, where it is believed that $\mu_n\tau_n > \mu_p\mu_p$, positive charge would build up near the cathode, as the electrons are swept out of the region adjacent to the cathode and the less mobile holes are left behind. In the reverse case, with $\mu_n\tau_n < \mu_p\mu_p$, negative charge will build up near the anode. Either case leads to a disproportionate amount of the applied voltage being dropped across the region where significant charge is accumulated. Goodman and Rose[42] use a simplified model to describe this problem for the case $\mu_n\tau_n < \mu_p\mu_p$. They assume that a photoconductor in a sandwich geometry is divided into three regions: near the anode (region 1), near the cathode (region 3), and in the center of the photoconductor (region 2). The widths of the regions near the anode and cathode are given by the mean drift length of the minority carrier (since it must be able to pass through each of the regions without recombining). Since $\mu_n\tau_n < \mu_p\mu_p$, negative charge builds up in region 1, and therefore a disproportionate amount of the applied voltage drops across this region. It is assumed that recombination does not occur in either region 1 or region 3, and that in region 2 recombination and generation are balanced. This model is applicable for voltages below V_0, at which the current density saturates to the value J_0. The current density and voltage variables, J and V, respectively, are converted to the dimensionless variables $j=J/J_0$, and $v=V/V_0$. The Goodman and Rose model predicts[42]

$$j = \frac{(1+b)\{-b+[b^2+4(1-b)(1+b^2)\mathrm{v}/(1+b)^2]^{1/2}\}}{2(1-b)}, \tag{6}$$

where

$$b \equiv \frac{\mu_n\tau_n}{\mu_p\tau_p}.$$

Equation (6) still holds true for the case in which $\mu_n\tau_n > \mu_p\mu_p$, except that the b in Eq. (6) must be replaced with $\beta=1/b$.

We modify the Goodman and Rose model to allow for field-dependent generation rates (i.e., ionization efficiencies) by allowing each of the three regions to have different generation rates, defined as g_1, g_2, and g_3. Furthermore, it is assumed that the generation rates in each region saturate to the same value, g_{sat} at high fields. This allows for a modification of Eq. (6) as follows:

$$j = \frac{\varepsilon_{1s}(1+b)\{-b\varepsilon_{12}+[b^2{\varepsilon_{12}}^2+4\mathrm{v}(1+b^2)(1-b\varepsilon_{12}+b^2{\varepsilon_{13}}^2-b^2\varepsilon_{12}\varepsilon_{13})/(1+b)^2]^{1/2}\}}{2(1-b\varepsilon_{12}+b^2{\varepsilon_{13}}^2-b^2\varepsilon_{12}\varepsilon_{13})}, \tag{7}$$

where b is still defined as in Eq. (6), and $\varepsilon_{1s}=g_1/g_{\mathrm{sat}}$, $\varepsilon_{12}=g_1/g_2$, and $\varepsilon_{13}=g_1/g_3$. If $\varepsilon_{1s}=\varepsilon_{12}=\varepsilon_{13}=1$, Eq. (7) reduces to Eq. (6).

It is assumed that the generation rate in each region follows the same field-dependence. Since we use our model only as a qualitative tool to understand the effect of field-dependent generation rates, a simple dependence that rises to a maximum is chosen:

$$g(E) = g_{\mathrm{sat}}(1-\exp(-E/E_s)), \tag{8}$$

where E_s defines how strongly the generation rate depends on field. Introducing field-dependent generation rates results in a problem that cannot be solved analytically, since the g_i depends on the field E_i in region i, and E_i depends on g_i. Instead, we solve the problem iteratively, using Eq. (6) to determine starting values for E_1, E_2, and E_3, which in turn determines the starting values for g_1, g_2, and g_3. These are then used for the calculation of j at the subsequent voltage step.

The solid line in Fig. 9 is the result of the iterative solution to Eq. (7), given a value for b of 0.6 and $E_s=0.7\ V_0/L$. Because Eq. (7) is not valid for $V>V_0$, we use a horizontal line to represent the photocurrent after saturation. The open circles in Fig. 9 represent photocurrent data for a sample treated with butylamine and dried at 70 °C, with the current and voltage scaled for comparison. The *j*-*v* curve represented by the solid line in Fig. 9 qualitatively reproduces the *i*-*V* curves of the amine- and base-treated samples: at low voltages, the photocurrent is highly voltage dependent, because of the voltage dependence of the generation rate; at voltages corresponding to $E>E_s$, the photocurrent becomes linear in voltage; and finally, at very high voltages the photocurrent saturates. In addition, the simulation shows that the nonzero voltage intercept of the linear region of the *i*-*V* curves is the result of having blocking electrodes that produce a build-up

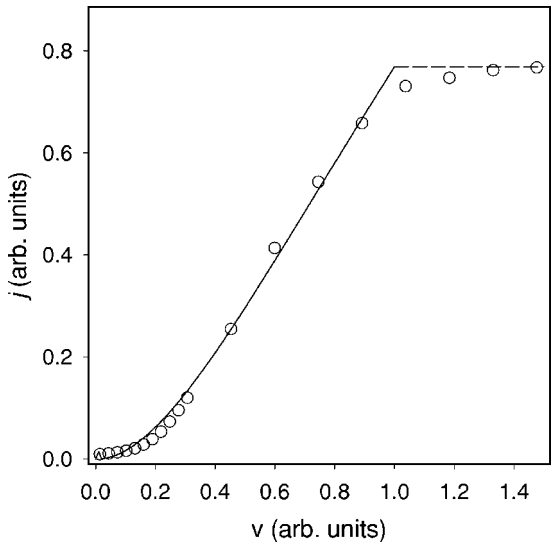

FIG. 9. Simulation of the current-voltage characteristics (solid line) for a photoconductor in a sandwich structure with two mobile carriers, noninjecting electrodes, and a field-dependent generation rate. For this simulation, the field characterizing the generation rate saturation is set to 0.7 times the field characterizing the current saturation. The ratio of $\mu\tau$ for the two carriers is set to 0.6. The simulation breaks down at saturation, at which point the current is given by the horizontal dashed line. For comparison, photocurrent data (open circles) for a sample treated with butylamine and dried at 70 °C are also presented. The current and voltage are scaled so that both are equal to one when the photocurrent saturates. The data are meant to be qualitatively compared to the simulation, since the simulation is not a result of a fit to the data.

of positive charge near the cathode, and of having a field-dependent exciton ionization efficiency.

It also seems clear from the simulation that the $\mu\tau$ products for holes and electrons in films of CdSe QDs may not be as different from each other as has been previously proposed.[45] For values of b less than ~ 0.1, the simulated j-v curve displays $j \propto v^{1/2}$ behavior at voltages that are far lower than what is observed for Fig. 1(b) and Fig. 4. This suggests that $\mu_n \tau_n$ probably does not exceed 10 times $\mu_p \tau_p$ in these films. It is not possible to determine whether this is also true for the other treated samples, since they do not exhibit saturation, and thus there is no reference voltage for a comparison to Fig. 9.

However, even for the samples that do exhibit a clear saturation, one should be cautious when drawing quantitative conclusions from the simulation based on the Goodman and Rose model because there are a several limitations. First, the field dependence for the generation rate in Eq. (8) is chosen for convenience, and is simpler than the actual field dependence. Second, the physics of the Goodman and Rose model is based on a photoconductor in a sandwich geometry, whereas the measurements presented here are for a planar geometry with a gate electrode. Third, the Goodman and Rose model simplifies the problem by defining three distinct regions within the photoconductor, when in reality the boundaries between the regions are not so abrupt. Nevertheless, the simulation provides important context for understanding the physics in our measurements.

The simulation also helps to explain the differences in the shapes of the i-V curves for the different types of samples measured. As E_s decreases, the simulated j-v curve in Fig. 9 shows that the transition to a linear regime also occurs at lower voltages. Comparing with experiment, this implies that unity ionization efficiency is achieved at lower voltages, for example for the sample treated with butylamine followed by drying at 70 °C than for the sample treated with butylamine and dried overnight.

The changes in the photocurrent behavior for the amine- and base-treated samples, compared to the reference samples, can now clearly be attributed to a substantial increase in the exciton ionization efficiency. The latter results from a competition between field ionization and recombination, radiative or nonradiative, within the QD. Thus, the ionization efficiency depends on both the exciton lifetime (with no applied voltage) and the distance between neighboring QDs, which influences the ionization rate.

The effect of distance is seen by comparing Fig. 1(a), the sample treated with butylamine and dried overnight, and Fig. 1(b), the sample treated with butylamine and dried at 70 °C. The chemical treatement in each case is the same, so the main difference is that the QDs are 4.6 Å apart for the sample in Fig. 1(a), and only 1.9 Å apart for the sample in Fig. 1(b). Bringing the QDs closer together increases the rate of electron tunneling between QDs and therefore increases the ionization efficiency.

The effect of exciton lifetime (with no applied field) can be seen by comparing Fig. 1(c), the sample treated with aniline, and Fig. 1(d), the sample treated with tri-*n*-butylphosphine (TBP). In each case, the QD spacing is the same, so the main difference is the functionality of the reagent used for treatment. Amines (and a basic environment in general) are known to increase quantum yield[25,36–40] by decreasing the rate of nonradiative exciton recombination through surface passivation. Since decreasing the rate of nonradiative exciton recombination makes the rate of ionization more competitive, it also increases the ionization efficiency.

Comparing the i-V curves in Figs. 1(a), 1(c), and 1(f) confirms the above assertions. AFM and GAXS analysis suggests that the QD spacing after treatment with butylamine [dried overnight; Fig. 1(a)], aniline [Fig. 1(c)], and 1,4-phenylenediamine [Fig. 1(f)] are all $\sim 6-8$ Å. The fact that all of these treatments result in similar improvements in photoconductivity and similar changes in the shapes of the i-V curves confirm that these effects are predominantly the result of the passivating nature of the amine functionality. Whether or not the amines used for treatment are conjugated or are diamines capable of cross-linking does not appear to have a strong effect. As expected, treatment with 1,6-diaminohexane results in a similar i-V curve that reaches a linear regime at slightly lower voltage than the other amine treatments, since the QD spacing is reduced to 4.1 Å.

Previous studies[26] have shown that the photoconductivity in CdSe QD films decreases with increasing temperature. This has been attributed to the increase in the nonradiative exciton recombination rate at higher temperatures, which leads to a decrease in exciton ionization efficiency for a given voltage. Figure 8(a) shows that the photocurrent for a

reference sample at 100 V is more than 30 times smaller at 300 K than it is at 77 K, consistent with previous observations. Figure 8(b) shows that the photocurrent at 100 V for a sample treated with butylamine and dried at 70 °C is only about 5 times smaller at 300 K than it is at 77 K. The weaker dependence of the photocurrent on temperature as well as the relative shapes of the *i*-*V* curves at 77 K and 300 K for the treated sample are consistent with the above model. Because of the increase in the nonradiative exciton recombination rate at 300 K, the *i*-*V* curve of the treated sample enters the linear regime, indicative of unity ionization efficiency, at a higher voltage at 300 K than at 77 K. Furthermore, while the treated *i*-*V* curve at 77 K saturates at 100 V, saturation is not observed at 300 K. This is because the photocurrent at 300 K is not as high as at 77 K, and according to Eq. (3) saturation should occur at a given current rather than a given voltage, independent of temperature.

V. CONCLUSIONS

Photoconductivity of CdSe QD films can be increased by postdeposition treatment with butylamine, aniline, 1,6-diaminohexane, 1,4-phenylenediamine, tri-*n*-butylphosphine, and sodium hydroxide. The *i*-*V* characteristics of the films after treatment confirm that the mechanism for improvement is an increase in the exciton ionization efficiency, which is achieved by increased QD surface passivation (due to the basic nature of amines and sodium hydroxide) and decreased QD spacing. For treatment with all of the amines and with sodium hydroxide, unity exciton ionization efficiency is attained. Furthermore, after treatment with sodium hydroxide or butylamine (when the sample is dried in the oven), the QD spacing is reduced enough for the photoconductivity to saturate at high voltage. This saturation is consistent with a model in which the electron lifetime becomes transit-time limited because there are two mobile carriers that are not replenished at the electrodes. We have presented a model that qualitatively reproduces the *i*-*V* characteristics of the amine- and base-treated samples by assuming blocking contacts and field-dependent generation rates (i.e., ionization efficiencies) that saturate at a voltage below the voltage necessary for photocurrent saturation.

These results and conclusions have important consequences for the potential use of CdSe QDs for optoelectronic applications such as photodetectors or solar cells. In addition to providing a method for achieving significant photocurrent at 77 K and room temperature for the first time, our results imply that photocurrent cannot be increased further unless electron and hole injection from the electrodes is facilitated. Potential methods to aid in carrier injection include: using a lower work function metal for the electrodes (for instance calcium or aluminum); converting from a lateral to a vertical structure so that another semiconductor could be introduced between the QDs and the electrodes in order to produce a gradient for electron and hole injection; and choosing another type of semiconductor QD with conduction and valence levels that align more favorably with the work function of gold.

ACKNOWLEDGMENTS

The authors would like to thank Joseph Adario and Peter Kloumann for their assistance with glancing angle x-ray diffraction. M.A.K. would also like to acknowledge discussions with H. Fritzsche about analogous experiments in amorphous semiconductors. This work was funded in part by the NSF-MRSEC program (DMR 0213282) at MIT and made use of its shared user facilities, and by the U.S. Army through the Institute for Soldier Nanotechnologies, under Contract No. DAAD-19-02-0002 with the U.S. Army Research Office.

[1] M. Dahan, S. Levi, C. Luccardini, P. Rostaing, B. Riveau, and A. Triller, Science **302**, 442 (2003).
[2] D.R. Larson, W.R. Zipfel, R.M. Williams, S.W. Clark, M.P. Bruchez, F.W. Wise, and W.W. Webb, Science **300**, 1434 (2003).
[3] J.K. Jaiswal, H. Mattoussi, J.M. Mauro, and S.M. Simon, Nat. Biotechnol. **21**, 47 (2003).
[4] B. Dubertret, P. Skourides, D.J. Norris, V. Noireaux, A.H. Brivanlou, and A. Libchaber, Science **298**, 1759 (2002).
[5] S. Kim, Y.T. Lim, E.G. Soltesz, A.M. De Grand, J. Lee, A. Nakayama, J.A. Parker, T. Mihaljevic, R.G. Laurence, D.M. Dor, L.H. Cohn, M.G. Bawendi, and J.V. Frangioni, Nat. Biotechnol. **22**, 93 (2004).
[6] S. Coe-Sullivan, W.K. Woo, J.S. Steckel, M. Bawendi, and V. Bulovic, Org. Electron. **4**, 123 (2003).
[7] S. Coe, W.K. Woo, M.G. Bawendi, and V. Bulovic, Nature (London) **420**, 800 (2002).
[8] V.L. Colvin, M.C. Schlamp, and A.P. Alivisatos, Nature (London) **370**, 354 (1994).
[9] B.O. Dabbousi, M.G. Bawendi, O. Onitsuka, and M.F. Rubner, Appl. Phys. Lett. **66**, 1316 (1995).
[10] W.U. Huynh, J.J. Dittmer, N. Teclemariam, D.J. Milliron, A.P. Alivisatos, and K.W.J. Barnham, Phys. Rev. B **67**, 115326 (2003).
[11] W.U. Huynh, J.J. Dittmer, and A.P. Alivisatos, Science **295**, 2425 (2002).
[12] A.J. Nozik, Physica E (Amsterdam) **14**, 115 (2002).
[13] P. Bhattacharya, A.D. Stiff-Roberts, S. Krishna, and S. Kennerly, Int. J. High Speed Electron. Syst. **12**, 969 (2002).
[14] L.W. Ji, Y.K. Su, S.J. Chang, S.H. Liu, C.K. Wang, S.T. Tsai, T.H. Fang, L.W. Wu, and Q.K. Xue, Solid-State Electron. **47**, 1753 (2003).
[15] H.-J. Eisler, V.C. Sundar, M.G. Bawendi, M. Walsh, H.I. Smith, and V. Klimov, Appl. Phys. Lett. **80**, 4614 (2002).
[16] V.C. Sundar, H.-J. Eisler, and M.G. Bawendi, *Advanced Materials* (Weinheim, Germany, 2002), Vol. 14, p. 739.
[17] M. Nirmal, B.O. Dabbousi, M.G. Bawendi, J.J. Macklin, J.K. Trautman, T.D. Harris, and L.E. Brus, Nature (London) **383**, 802 (1996).
[18] W.K. Woo, K.T. Shimizu, M.V. Jarosz, R.G. Neuhauser, C.A. Leatherdale, M.A. Rubner, and M.G. Bawendi, Adv. Mater. (Weinheim, Ger.) **14**, 1068 (2002).

[19] M. Shim, C.J. Wang, and P. Guyot-Sionnest, J. Phys. Chem. B **105**, 2369 (2001).
[20] C.J. Wang, M. Shim, and P. Guyot-Sionnest, Science **291**, 2390 (2001).
[21] M.A. Kastner, Phys. Today **46**, 24 (1993).
[22] M. Drndic, M.V. Jarosz, N.Y. Morgan, M.A. Kastner, and M.G. Bawendi, J. Appl. Phys. (unpublished).
[23] P. Guyot-Sionnest and C. Wang, J. Phys. Chem. B **107**, 7355 (2003).
[24] D. Yu, C.J. Wang, and P. Guyot-Sionnest, Science **300**, 1277 (2003).
[25] B.K.H. Yen, N.E. Stott, K.F. Jensen, and M.G. Bawendi, Adv. Mater. (Weinheim, Ger.) **15**, 1858 (2003).
[26] C.A. Leatherdale, C.R. Kagan, N.Y. Morgan, S.A. Empedocles, M.A. Kastner, and M.G. Bawendi, Phys. Rev. B **62**, 2669 (2000).
[27] C.B. Murray, D.J. Norris, and M.G. Bawendi, J. Am. Chem. Soc. **115**, 8706 (1993).
[28] C.B. Murray, C.R. Kagan, and M.G. Bawendi, Science **270**, 1335 (1995).
[29] C.B. Murray, C.R. Kagan, and M.G. Bawendi, Annu. Rev. Mater. Sci. **30**, 545 (2000).
[30] M.V. Jarosz, N.E. Stott, M. Drndic, N.Y. Morgan, M.A. Kastner, and M.G. Bawendi, J. Phys. Chem. B **107**, 12 585 (2003).
[31] C.R. Kagan, C.B. Murray, and M.G. Bawendi, Phys. Rev. B **54**, 8633 (1996).
[32] C.R. Kagan, C.B. Murray, M. Nirmal, and M.G. Bawendi, Phys. Rev. Lett. **76**, 1517 (1996).
[33] N.Y. Morgan, C.A. Leatherdale, M. Drndic, M.V. Jarosz, M.A. Kastner, and M. Bawendi, Phys. Rev. B **66**, 075339 (2002).
[34] C. Kagan, Ph.D. thesis, Massachusetts Institute of Technology, 1996.
[35] B.E. Warren, *X-Ray Diffraction* (Addison-Wesley, Reading, 1969).
[36] L. Spanhel, M. Haase, H. Weller, and A. Henglein, J. Am. Chem. Soc. **109**, 5649 (1987).
[37] D.V. Talapin, A.L. Rogach, I. Mekis, S. Haubold, A. Kornowski, M. Haase, and H. Weller, Colloids Surf., A **202**, 145 (2002).
[38] W.-K. Woo, Ph.D. thesis, Massachusetts Institute of Technology, 2002.
[39] X.G. Peng, M.C. Schlamp, A.V. Kadavanich, and A.P. Alivisatos, J. Am. Chem. Soc. **119**, 7019 (1997).
[40] D.V. Talapin, A.L. Rogach, A. Kornowski, M. Haase, and H. Weller, Nano Lett. **1**, 207 (2001).
[41] R.H. Bube, *Photoconductivity of Solids* (Wiley, New York, 1960).
[42] A.M. Goodman and A. Rose, J. Appl. Phys. **42**, 2823 (1971).
[43] A. Rose, *Concepts in Photoconductivity and Allied Problems*, Interscience Tracts on Physics and Astronomy, edited by R.E. Marshak (Interscience, London, 1963).
[44] F.C. Nix, Rev. Mod. Phys. **4**, 723 (1932).
[45] D.S. Ginger and N.C. Greenham, J. Appl. Phys. **87**, 1361 (2000).
[46] H. Mattoussi, L.H. Radzilowski, B.O. Dabbousi, E.L. Thomas, M.G. Bawendi, and M.F. Rubner, J. Appl. Phys. **83**, 7965 (1998).